A "Dendritic Effect" in Homogeneous Catalysis with Carbosilane-Supported Arylnickel(II) Catalysts: Observation of Active-Site Proximity Effects in Atom-Transfer Radical Addition

Arjan W. Kleij,[†] Robert A. Gossage,[†,⊥] Robertus J. M. Klein Gebbink,[†] Nils Brinkmann,[‡] Ed J. Reijerse,[∥] Udo Kragl,[‡] Martin Lutz,[§] Anthony L. Spek,[§,#] and Gerard van Koten*[,†]

Contribution from the Debye Institute, Department of Metal-Mediated Synthesis, Utrecht University, Padualaan 8, 3584 CH, Utrecht, The Netherlands, Forschungszentrum Jülich GmbH, Institut für Biotechnologie, D-52425 Jülich, Germany, Bijvoet Center for Biomolecular Research, Department of Crystal and Structural Chemistry, Utrecht University, Padualaan 8, 3584 CH Utrecht, The Netherlands, Department of Molecular Spectroscopy, University of Nijmegen, Toernooiveld, 6525 ED, Nijmegen, The Netherlands

Received July 19, 2000

Abstract: Transmetalation of polylithiated, carbosilane (CS) dendrimers functionalized with the potentially terdentate ligand $[C_6H_2(CH_2NMe_2)_2$-2,6-R-4$]^-$ (= NCN) with $NiCl_2(PEt_3)_2$ produced a series of nickel-containing dendrimers [G0]-Ni_4 (**4**), [G1]-Ni_{12} (**5**), and [G2]-Ni_{36} (**7**) in moderate to good yields. The metallodendrimers **4**, **5**, and **7** are catalytically active in the atom-transfer radical addition (ATRA) reaction (Kharasch addition reaction), viz. the 1:1 addition of CCl_4 to methyl methacrylate (MMA). The catalytic data were compared to those obtained for the respective mononuclear compound $[NiCl(C_6H_2\{CH_2NMe_2\}_2$-2,6-$SiMe_3$-4)] (**2**). This comparison indicates a fast deactivation for the dendrimer catalysts beyond generation [G0]. The deactivation of [G1]-Ni_{12} (**5**) and [G2]-Ni_{36} (**7**) is caused by irreversible formation of catalytically inactive Ni(III) sites on the periphery of these dendrimers. This hypothesis is supported by results of model studies as well as ESR spectroscopic investigations. Interestingly, the use of two alternative nickelated [G1] dendrimers [G1]*-Ni_{12} (**11**) and [G1]-Ni_8 (**15**), respectively, in which the distance between the Ni sites is increased, leads to significantly improved catalytic efficiencies which approximate those of the parent derivative **2** and [G0]-Ni_4 (**4**). Preliminary membrane catalysis experiments with [G0]-Ni_4 (**4**) and [G1]-Ni_{12} (**5**) show that **5** can be efficiently retained in a membrane reactor system. The X-ray crystal structure of the Ni(III) complex $[NiCl_2(C_6H_2\{CH_2NMe_2\}_2$-2,6-$SiMe_3$-4)] (**16**), obtained from the reaction of **2** with CCl_4, is also reported.

Introduction

Current research in our group concentrates on the use of (carbosilane) dendrimers[1−4] and hyperbranched polymers[5] to create new materials that bridge the gap between homogeneous and heterogeneous catalysis. In this regard, we pioneered the first "metallodendrimer catalyst", in which catalytically active metal centers were connected to an inert carbosilane framework via an appropriate (carbamate) linker group (see Figure 1).[6] These compounds were designed to take advantage of the activity, selectivity, and ease of characterization and modification of homogeneous catalysts in combination with the size properties that are necessary for effective recovery (i.e., nanofiltration) of the catalytic species (cf., heterogeneous systems).[3b,7]

* To whom correspondence should be adressed. Telephone: +3130 2533120. Fax: +3130 2523615. E-mail: g.vankoten@chem.uu.nl.

[†] Department of Metal-Mediated Synthesis, Utrecht University.

[‡] Institut für Biotechnologie.

[§] Department of Crystal and Structural Chemistry, Utrecht University.

[∥] University of Nijmegen.

[⊥] Current address: Department of Chemistry, Acadia University, Wolfville, Novia Scotia, Canada BOP1XO.

[#] Address correspondence pertaining to crystallographic studies to this author. E-mail: a.l.spek@chem.uu.nl.

(1) For reviews on this subject, see: (a) Newkome, G.; Moorefield, C. N.; Vögtle, F. *Dendritic Molecules - Concepts, Syntheses, Perspectives*; VCH: Weinheim, 1996. (b) Newkome, G., Ed. *Advances in Dendritic Macromolecules*; JAI Press: Greenwich, CT, 1995. For more recent reviews in dendrimer chemistry, see: (c) Bosman, A. W.; Janssen, H. M.; Meijer, E. W. *Chem. Rev.* **1999**, *99*, 1665. (d) Newkome, G.; He, E.; Moorefield *Chem. Rev.* **1999**, *99*, 1689. (e) Fischer, M.; Vögtle, F. *Angew. Chem., Int. Ed.* **1999**, *38*, 885 (f) Frey, H.; Lach, C.; Lorenz, K. *Adv. Mater.* **1998**, *10*, 279. (g) Gorman, C. *ibid.* **1998**, *10*, 295. (h) Gudat, D. *Angew. Chem., Int. Ed. Engl.* **1997**, *36*, 1951. (i) Fréchet, J. M. J.; Hawker, C. J.; Gitsov, I.; Leon, J. W. *J. Macromol. Sci. Pure Appl. Chem.* **1996**, *A33*, 1399. Dendritic compounds have been made primarily from carbon-based materials, although the "branching points" are frequently heteroatoms such as nitrogen[2], phosphorus,[3] and silicon.[4]

(2) (a) Tomalia, D. A.; Taylor, A. M.; Goddard, W. A., III. *Angew. Chem.* **1990**, *102*, 119−156, *Angew. Chem., Int. Ed. Engl.* **1990**, *29*, 138−175. (b) Tomalia, D. A. *Sci. Am.* **1995**, *272*, 62−70.

(3) (a) Majoral, J. P.; Caminade, A. M. *Chem. Rev.* **1999**, *99*, 845−880 and references therein. (b) de Groot, D.; Eggeling, E. B.; de Wilde, J. C.; Kooijman, H.; Haaren, R. J.; van der Made, A. W.; Spek, A. L.; Vogt, D.; Reek, J. N. H.; Kamer, P. C. J.; van Leeuwen, P. W. N. M. *Chem. Commun.* **1999**, 1623. (c) Petrucci-Samija, Guillemette, V.; Dasgupta, M.; Kakkar, A. K. *J. Am. Chem. Soc.* **1999**, *121*, 1968. (d) Alper, H.; Bourque, S. C.; Manzer, L. E.; Arya, P. *J. Am. Chem. Soc.* **2000**, *122*, 956.

(4) (a) van der Made, A. W.; van Leeuwen, P. W. N. M. *J. Chem. Soc., Chem. Commun.* **1992**, 1400−1401. (b) Zhou, L. L.; Roovers, J. *Macromolecules* **1993**, *26*, 963−968. (c) Roovers, J.; Zhou, L. L.; Toporowski, P. M.; van der Zwan, M.; Iatrou, H.; Hadjichristidis, N. *ibid.* **1993**, *26*, 4324−4329. (d) van der Made, A. W.; van Leeuwen, P. W. N. M.; de Wilde, J. C.; Brandes, R. A. C. *Adv. Mater.* **1993**, *5*, 466−468.

(5) Schlenk, C.; Kleij, A. W.; Frey, H.; van Koten, G. *Angew. Chem., Int. Ed.* **2000**, *39*, 3445−3447.

(6) Knapen, J. W. J.; Van der Made, A. W.; de Wilde, J. C.; van Leeuwen, P. W. N. M.; Wijkens, P.; Grove, D. M.; van Koten, G. *Nature* **1994**, *372*, 659−663.

10.1021/ja0026612 CCC: $19.00
Published on Web 11/22/2000

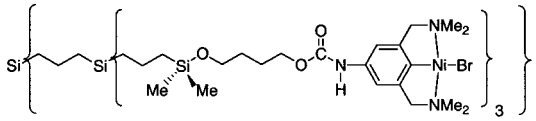

Figure 1. Schematic representation of a metallodendritic catalyst.[6]

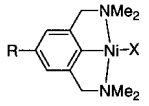

Figure 2. Schematic structure of *para*-functionalized nickel complexes derived from the NCN ligand.

The original dendrimer catalysts gave comparable activity per metal atom when compared with the monomeric analogues (Figure 2, X = Br).[8] Specifically, these Ni-based complexes are active catalysts for the atom-transfer radical (i.e., Kharasch) addition of polyhalogenated alkanes to olefins[9] and are characterized by the incorporation of a bis(*ortho*) chelating monoanionic "pincer" ligand. This fragment contains a formal aryl carbanion in combination with two trans-positioned tertiary amine donor groups and is derived from the simple *para*-substituted arenes 1-R-3,5-bis[(dimethylamino)methyl]benzene (Figure 2).[8] Ligands of this class are currently an area of active study due to the unique catalytic properties of a variety of metal "pincer" complexes.[10]

In this report, we detail a novel synthetic methodology for the production of metallodendrimer catalysts via a simple procedure involving attachment of the "pincer" ligand to the dendrimer periphery via a Si−C bond. The resulting pincer-containing, dendrimer ligands were selectively lithiated and transmetalated,[11] affording catalytic units which are bound to the dendritic framework via a direct Si−C bond. This latter feature makes the metallodendrimers chemically even more robust than our earlier systems (Figure 1). However, removal of the carbamate-based linker will dramatically affect the nature of the sterical crowding at the periphery of the CS-dendritic species and, in particular, the mutual distance between the Ni catalytic sites. We have further explored the catalytic activity of these new metallodendrimers in the atom-transfer radical addition reaction and compared the turnover numbers and electrochemical properties of these materials with the respective mononuclear analogue [NiCl(C_6H_2\{CH_2NMe_2\}$_2$-2,6-R-4)] (Figure 2, R = $SiMe_3$).

In an earlier preliminary communication, we have reported that the higher-generation metallodendritic catalysts have dramatically lower catalytic activities and that the Ni sites no longer act as independent catalytic units.[12] However, it was also shown that an increase in spatial separation between the nickel sites brought about by the use of sterically less congested CS-dendritic supports, led to retention of catalytic activity. The underlying mechanistic reasons for the deactivation of the higher-generation nickel-containing dendrimers have been studied in more detail and are described herein. Moreover, recent results demonstrate that modern ultrafiltration membrane reactors can be used to effectively recover the dendrimer catalysts and hence can be employed for continuous-operation applications in homogeneous catalysis.[13]

Results and Discussion

Preparation of Nickelated Carbosilane Dendrimers. Recently, we reported the synthesis of carbosilane dendrimers functionalized with terminal bidentate (C,N) or tridentate (N,C,N) ligand fragments.[11] These systems could be selectively and quantitatively converted into their corresponding polylithiated analogues. We anticipated that these lithiated carbosilanes would be useful starting materials for the synthesis of metallodendrimers containing various (N)CN-ligated transition metal fragments. Therefore, we extended these earlier studies and prepared a series of novel nickel-containing carbosilane dendrimers with the NCN−NiCl fragments attached to the dendritic backbone via a direct, stable Si−C bond. We prepared the model compounds [NiCl(C_6H_2\{CH_2NMe_2\}$_2$-2,6-$SiMe_3$-4)] (**2**) and Me_2Si[C_6H_2\{CH_2NMe_2\}$_2$-3,5-(NiCl)-4]$_2$ (**3**) to serve as reference compounds in catalysis and for electrochemical investigations using cyclic voltammetry.

The mono-nickelated derivative [NiCl(C_6H_2\{CH_2NMe_2\}$_2$-2,6-$SiMe_3$-4)] (**2**) was obtained by a two-step reaction sequence. Lithiation of 1-trimethylsilyl-3,5-bis[(dimethylamino)methyl]-benzene[14] with **t**-BuLi in hexane at room temperature (RT) for 18 h, followed by treatment of the lithiated intermediate with [$NiCl_2(PEt_3)_2$][15] affords **2** as an orange solid (61% yield). The bis-nickelated derivative Me_2Si[C_6H_2\{CH_2NMe_2\}$_2$-3,5-(NiCl)-4]$_2$ (**3**) was produced in a 66% yield by a similar approach using the silane derivative Me_2Si[C_6H_3\{CH_2NMe_2\}$_2$-3,5]$_2$ (**1**) as starting material. This latter compound was obtained as a yellow oil and isolated in quantitative yield by treatment of Me_2SiCl_2 with an excess of the lithium reagent [Li(C_6H_3\{CH_2NMe_2\}$_2$-3,5)][11a] (= Li−NCN, Scheme 1). The dendrimer analogues of

(7) (a) Hovestad, N. J.; Eggeling, E. B.; Heidbüchel, H. J.; Jastrzebski, J. T. B. H.; Kragl, U.; Keim, W.; Vogt, D.; van Koten, G. *Angew. Chem., Int. Ed.* **1999**, *111*, 1763. (b) Brinkmann, N.; Giebel, D.; Lohmer, G.; Reetz, M. T.; Kragl, U. *J. Catal.* **1999**, *183*, 163−168. (c) Giffels, G.; Beliczey, J.; Felder, M.; Kragl, U. *Tetrahedron: Assymmetry* **1998**, *9*, 691−696.

(8) (a) van de Kuil, L. A.; Luitjes, H.; Grove, D. M.; Zwikker, J. W.; van de Linden, J. G. M.; Roelofsen, A. M.; Jenneskens, L. W.; Drenth, W.; van Koten, G. *Organometallics* **1994**, *13*, 468−477. (b) Grove, D. M.; Verschuuren, A. H. M.; van Koten, G. *J. Mol. Catal.* **1988**, *45*, 169. (c) Grove, D. M.; Verschuuren, A. H. M.; van Koten, G.; van Beek, J. A. M. *J. Organomet. Chem.* **1989**, *372*, C1−C6.

(9) (a) Gossage, R. A.; van de Kuil, L. A.; van Koten, G. *Acc. Chem. Res.* **1998**, *31*, 423. (b) van de Kuil, L. A.; Grove, D. M.; Gossage, R. A.; Zwikker, J. W.; Jenneskens, L. W.; Drenth, W.; van Koten, G. *ibid.* **1997**, *16*, 4985−4994. (c) Kharasch, M. S.; Jensen, E. V.; Urry, W. H. *Science* **1945**, *102*, 128.

(10) For *NCN*-type ligands, see: (a) van Koten, G. *Pure Appl. Chem.* **1989**, *61*, 1681−1694. (b) Rietveld, M. H. P.; Grove, D. M.; van Koten, G. *New J. Chem.* **1997**, *21*, 751−771. (c) Stark, M. A.; Jones, G.; Richards, C. J. *Organometallics* **2000**, *19*, 1282. For *PCP*-type ligands, see: (d) Dani, P.; Karlen, T.; Gossage, R. A.; Gladiali, S.; van Koten, G. *Angew. Chem., Int. Ed.* **2000**, *39*, 743. (e) Gupta, M.; Hagen, C.; Kaska, W.; Cramer, R. E.; Jensen, C. M. *J. Am. Chem. Soc.* **1997**, *119*, 840. (f) Lee, D. W.; Kaska, W. C.; Jensen, C. M. *Organometallics* **1998**, *17*, 1. (g) Jensen, C. M. *Chem. Commun.* **1999**, 2443. (h) Liu, F.; Goldman, A. S. *Chem. Commun.* **1999**, 655. (i) Longmire, J. M.; Zhang, X. *Organometallics* **1998**, *17*, 4374. (j) Gorla, F.; Togni, A.; Venanzi, L. M.; Albinati, A.; Lianza, F. *Organometallics* **1994**, *13*, 1607. For *SCS*-type ligands, see: (k) Loeb, S. J.; Shimizu, G. K. H. *J. Chem. Soc., Chem. Commun.* **1993**, 1395. (l) Moulton, C. J.; Shaw, B. L. *J. Chem. Soc., Dalton Trans.* **1975**, 1020. (m) Bergbreiter, D. E.; Osburn, P. L.; Liu, Y.-S. *J. Am. Chem. Soc.* **1999**, *121*, 9531. For a review on C−C bond activation by "pincer" type complexes, see: (n) Rybtchinski, B.; Milstein, D. *Angew. Chem., Int. Ed.* **1999**, *38*, 870.

(11) (a) Kleij, A. W.; Klein, H.; Jastrzebski, J. T. B. H.; Smeets, W. J. J.; Spek, A. L.; van Koten, G. *Organometallics* **1999**, *18*, 268. (b) Kleij, A. W.; Klein, H.; Jastrzebski, J. T. B. H.; Spek, A. L.; van Koten, G. *Organometallics* **1999**, *18*, 277.

(12) For a preliminary communication of this work, see: Kleij, A. W.; Gossage, R. A.; Jastrzebski, J. T. B. H.; Boersma, J.; van Koten, G. *Angew. Chem., Int. Ed.* **2000**, *39*, 179.

(13) (a) Kragl, U. and Dreisbach, C. *Angew. Chem., Int. Ed. Engl.* **1996**, *35*, 642. (b) Kragl, U.; Dreisbach, C.; Wandrey, C. Membrane reactors in Homogeneous Catalysis. *Applied Homogeneous Catalysis with Organometallic Compounds*; Cornils, B., Herrmann, W. A., Eds.; VCH: Weinheim, 1996; pp 833−843.

(14) Steenwinkel, P.; James, S. L.; Grove, D. M.; Veldman, N.; Spek, A. L.; van Koten, G. *Chem. Eur. J.* **1996**, *2*, 1440.

(15) This transmetallating reagent is easily prepared from the reaction between $NiCl_2 \cdot 6H_2O$ and PEt_3 in EtOH. See: Jensen, K. A. *Z. Anorg. Allg. Chem.* **1936**, *Band 229*, 273.

Scheme 1: Synthesis of Model Compounds **2** and **3**[a]

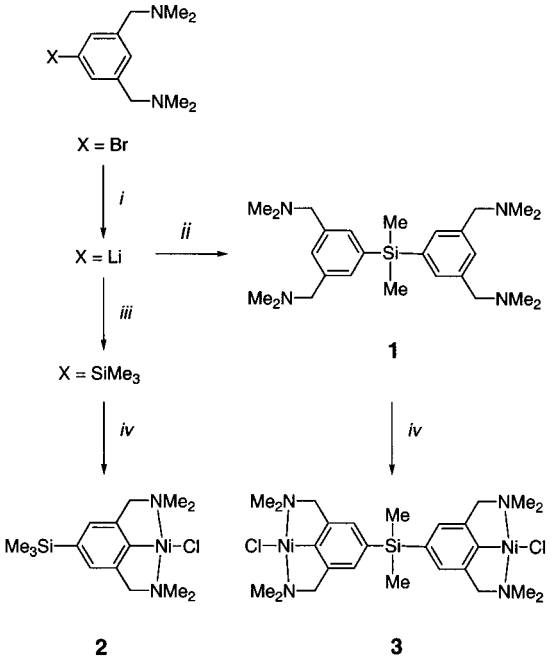

[a] *Reagents and conditions:* (i) 2 equiv *t*-BuLi, Et_2O, −78 °C; (ii) 0.5 equiv Me_2SiCl_2, Et_2O, -78 °C → RT; (iii) excess Me_3SiCl, Et_2O, 78 °C → RT; (iv) *t*-BuLi, pentane, RT; $NiCl_2(PEt_3)_2$, Et_2O.

2 and **3** were synthesized in moderate to good yields (32−86%) by the reaction of their polylithiated precursors with an appropriate amount of $[NiCl_2(PEt_3)_2]$ at RT as described below.

The synthesis of the metallodendrimers [G0]-Ni_4 (**4**), [G1]-Ni_{12} (**5**), and [G2]-Ni_{36} (**7**) (Schemes 2 and 3) began with the preparation of the polylithiated precursors of the dendritic ligand precursors [G0]-$SiMe_2$−NCN,[11a] [G1]-$SiMe_2$−NCN[11a] and [G2]-$SiMe_2$−NCN (**6**). The second generation NCN-functionalized carbosilane dendrimer **6** could be prepared in a moderate yield (48%) as an extremely viscous oil by treatment of the polychlorosilane [G2]-$SiMe_2Cl$[4a] with an excess of Li−NCN as described for the [G0]- and [G1]-generation derivatives (vide supra).[11a] The polylithiated reagents were obtained as amorphous, insoluble red solids by addition of excess of *t*-BuLi to these ligand systems and were subsequently purified by removing the excess *t*-BuLi by washing with dry hexanes. After this step, the transmetallating reagent (i.e., $[NiCl_2(PEt_3)_2]$) was added as a diethyl ether solution which afforded the multimetallic dendrimers **4**, **5**, and **7** after appropriate workup.

To no surprise, the use of these extremely moisture-sensitive lithium reagents typically resulted in partial hydrolysis during workup. As a result, we found that nickelation of the ligand sites beyond 80−90% could not be achieved.[17] Spectroscopic evidence for this is found in the ^1H and $^{13}C\{^1H\}$ NMR spectra of [G0]-Ni_4 (**4**), [G1]-Ni_{12} (**5**), and [G2]-Ni_{36} (**7**), in which signals that were attributed to nonmetalated NCN fragments, were clearly visible. A *single* resonance pattern is found for both metalated as well as non-nickelated NCN sites. The ^1H NMR spectroscopic signal integration of *all* NCN sites corresponded with the signal integration for the $SiMe_2$ groups of the CS-dendritic support. The microanalyses of **4**, **5**, and **7** were in agreement with the calculated percentage of metalation as obtained by ^1H NMR spectroscopy (i.e., signal integration). It should be noted that dendrimer [G2]-Ni_{36} (**7**) is *less* soluble than [G0]-Ni_4 (**4**) and [G1]-Ni_{12} (**5**), indicating that beyond the first generation the solubility behavior is increasingly controlled by the peripheral organometallic groups (i.e., size). The decreased solubility features found for **7** could explain its low isolated yield.

In addition, we also prepared two less "condensed" [G1] nickelated carbosilane dendrimers. These alternative [G1] dendrimers were constructed to be able to vary the proximity between the surface-bonded nickel sites and their accessibility for substrate molecules (vide infra).

Two different approaches were used to increase the separation between the external organonickel(II) chloride groups. The first approach involves the introduction of an inert carbosilane tether (i.e., $-CH_2CH_2CH_2Si(Me)_2-$) on the [G1] periphery. The synthetic pathway leading to the extended nickel-containing dendrimer **11** (abbreviated as [G1]*-Ni_{12}) is outlined in Scheme 4.

The synthesis of [G1]*-Ni_{12} (**11**) begins with an allylation reaction of the known chlorosilane [G1]-$SiMe_2Cl$[4a] with an excess of allylMgBr to yield the dodeca-olefin [G1]-$SiMe_2-CH_2CH{=}CH_2$ (**8**) as a viscous oil (88% yield). Compound **8** was quantitatively converted into [G1]-$C_3H_6-SiMe_2Cl$ (**9**) by hydrosilylation in the presence of a large excess of $HSiMe_2Cl$ using $[(NBu_4)_2PtCl_6]$ as catalyst. Treatment of **9** with an excess of Li−NCN[11a] afforded the extended dendrimer ligand [G1]-$C_3H_6-SiMe_2-$NCN (**10**) as a yellow, vicous oil in 87% yield. Finally, the nickelated derivative [G1]*-Ni_{12} (**11**) was prepared (50% yield) by a similar lithiation/transmetalation procedure as described earlier for **4**, **5**, and **7**. The moderate yield of **11** is probably a result of the increased solubility behavior of this compound. This rendered the purification and workup of **11** less efficient. The dendritic materials **8**−**11** were identified by ^1H, $^{13}C\{^1H\}$, and $^{29}Si\{^1H\}$ NMR spectroscopy, as well as by MALDI-TOF mass spectrometry and combustion analyses.

A second approach to increase the separation between the catalytic sites is depicted in Scheme 5 and was aimed at the introduction of *less* [G1] periphery-bonded nickel(II) complexes. This leads to the [G1] nickelated dendrimer **15** (abbreviated as [G1]-Ni_8), which was prepared in three consecutive steps. The carbosilane dendrimer species [G1]-$(CH_2CH{=}CH_2)_8$ (**12**) was prepared using a procedure described in the literature[4] and fully characterized[17] before its use in subsequent syntheses.

The first step in the synthesis of [G1]-Ni_8 (**15**) was the hydrosilylation of **12** in neat $HSiMe_2Cl$ under platinum catalysis as described for **9** (vide supra) which gave dendrimer [G1]-$(SiMe_2Cl)_8$ (**13**: 95% yield). The latter was immediately converted into the air stable dendrimer [G1]-$(NCN)_8$ (**14**) by treatment with an excess of Li−NCN as described for **10**. The nickelated dendrimer **15** was obtained as an orange solid in 79% yield by using a similar lithiation/transmetalation sequence as was used for **11**. The structures of **12**−**15** were confirmed by NMR spectroscopy (^1H, $^{13}C\{^1H\}$, and $^{29}Si\{^1H\}$), mass spectrometry (MALDI-TOF), and elemental analyses.

As for the other nickelated dendrimers, an incomplete metalation was observed for **11** and **15**. The percentage of nickel incorporation was estimated by ^1H NMR spectroscopy and elemental analyses and indicated a nickel loading for both dendrimers (**11**: 79%; **15**: 89%) falling in the same range as was established for **4**, **5**, and **7** (viz. 80−90%). These results clearly demonstrated the limitations but also the reproducibility of the lithiation/transmetalation sequence for introducing metal sites into this type of NCN-containing dendrimer.

Characterization of (Nickelated) Dendrimers: NMR Spectroscopy. As for the related model compounds **2** and **3**,[18] NMR

(16) We have found that similar transmetalation reactions with Pt^{II} salts gave comparable results.[12b]

(17) To our knowledge, no analytical data was available for this particular dendrimer.

Scheme 2: Synthesis of [G0] and [G1] Dendrimers **4** and **5**[a]

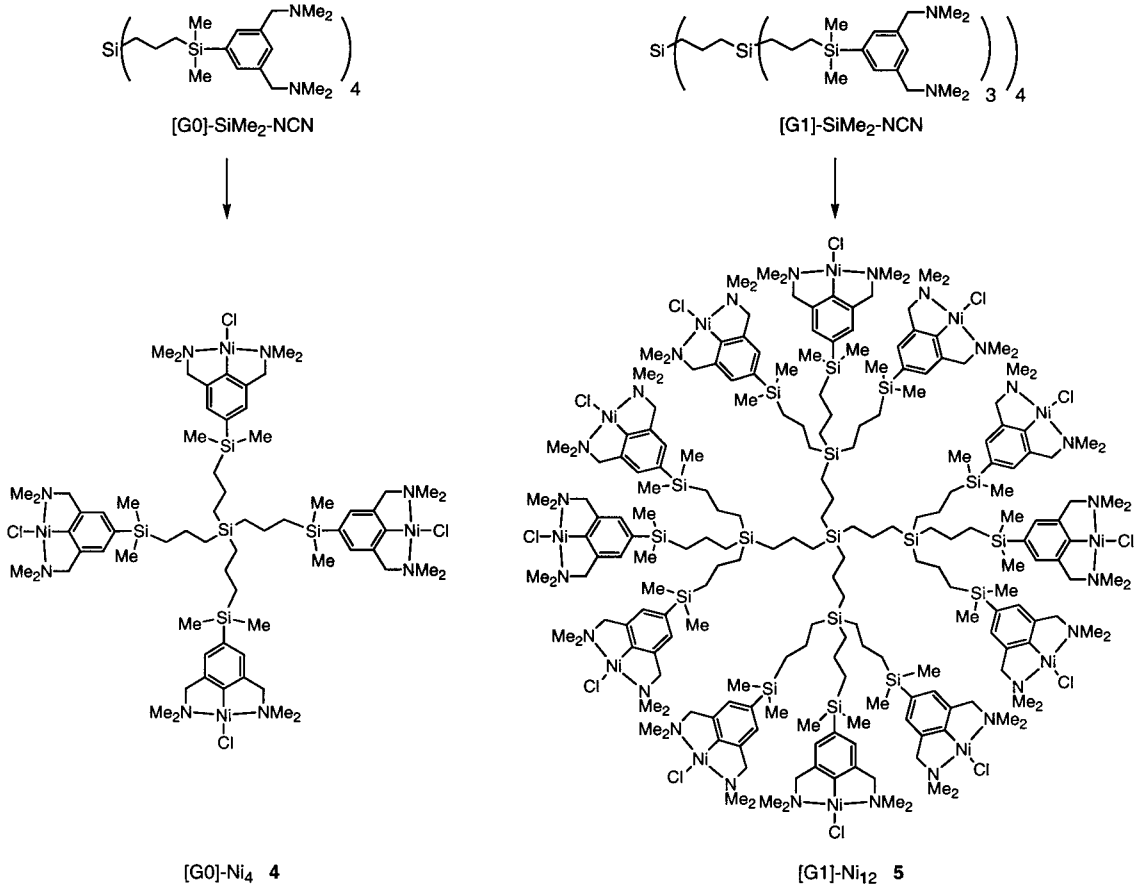

[a] *Reagents and conditions:* (i) *t*-BuLi, pentane, RT; $NiCl_2(PEt_3)_2$, Et_2O.

(^1H and $^{13}C\{^1H\}$) spectroscopic characterization of **4**-**15**[18] (C_6D_6; RT) revealed single resonances patterns for the CH_2N, $N(CH_3)_2$, and $Si(CH_3)_2$ groups. This result suggests free rotation for both the dendritic branches around the central Si (core) atom and the ligands located on the dendrimer periphery. Of particular note is that in the $^{13}C\{^1H\}$ NMR spectrum of **5**, the inner and periphery CH_2 fragments of the carbosilane skeleton gave rise to five separate resonances, while a theoretical sixth resonance is most probably coincident with one of the signals observed for the other methylenic groupings. In the 75 MHz $^{13}C\{^1H\}$ NMR spectrum obtained for the [G2] dendrimer ligand **6**; however, the signals corresponding for the methylenic carbon atoms are overlapped at this field, and as a result, only three broad peaks were observed. This suggests that the intramolecular rotational freedom in these dendrimer molecules decreases with increasing generation number. $^{29}Si\{^1H\}$ NMR spectroscopy proved to be a very helpful technique for a further structural assignment of **6**. This NMR spectrum showed four (expected) resonances at 1.48, 1.14, 0.75, and −3.76 ppm, respectively. Strangely, one additional resonance (δ = −3.07 ppm) is observed, and this could indicate the presence of structural defects present in **6**. This latter resonance is ascribed to a silicon center which is bonded to an aryl group. The observation of this extra resonance could be caused by the introduction of, for example, Markovnikov addition of $SiMe_2Cl$ groups, followed by arylation of the resulting β-SiCl groups. We estimated this defect to be present in only small amounts (∼4%) by means of signal integration.

The NMR spectra of the extended dendrimer ligand precursors **8**−**10** is likewise helpful for structural assignment. Of particular note is the $^{13}C\{^1H\}$ NMR spectrum of **8**, which displayed six separated resonances for the methylenic groups of the carbosilane support of which three were significantly smaller in intensity. The $^{29}Si\{^1H\}$ NMR spectrum of the same compound showed three distinctive resonances (δ = 1.10, 1.04, and 0.89 ppm, respectively). The hydrosilylation of **8** to give [G1]-C_3H_6−$SiMe_2Cl$ (**9**) could be easily monitored, as the resonances of the olefinic groups in the ^1H and $^{13}C\{^1H\}$ spectra of **8** disappeared with time. This was accompanied by the appearance of additional resonances assigned to new CH_2 and $Si(CH_3)_2$ groups. The $^{29}Si\{^1H\}$ NMR spectrum of **9** clearly showed the new signal (δ = 30.76 ppm) attributed to the introduced $SiMe_2$-Cl fragment. The NMR spectra recorded for [G1]-C_3H_6−$SiMe_2$−NCN (**10**) and [G1]*-Ni_{12} (**11**) showed an increased overlap between the different dendrimer segments and hence the presence of broader resonance patterns. Similar NMR spectroscopic observations were encountered for the dendrimer ligand precursors **12**−**14** and [G1]-Ni_8 (**15**).

Mass Spectrometric Analysis. Although all nickelated dendrimers are sensitive to oxidation, one can readily perform mass spectrometric analyses for the model derivatives **2**, **3**, and **4**. For this purpose, fast atom bombardment (FAB) mass spectrometry proved to be an effective method for analyzing these relatively small molecules. This procedure afforded spectra containing many ion clusters with well-resolved isotopic patterns. The FAB-MS spectra of **2**−**4** displayed characteristic

(18) The NMR spectra of the (nickelated dendrimer) species tend to suffer from line-broadening which is most likely caused by the presence of traces of paramagnetic Ni^{III}. To overcome this problem, NMR samples containing these compounds can be treated with CO(g) to reduce traces of Ni(III) *prior* to spectroscopic measurement which reduces the line-broadening. See: Grove, D. M.; van Koten, G.; Mul, W. P.; van der Zeijden, A. A. H.; Terheijden, J. *Organometallics* **1986**, *5*, 322−326.

Scheme 3: Synthesis of [G2] Dendrimers **6** and **7**[a]

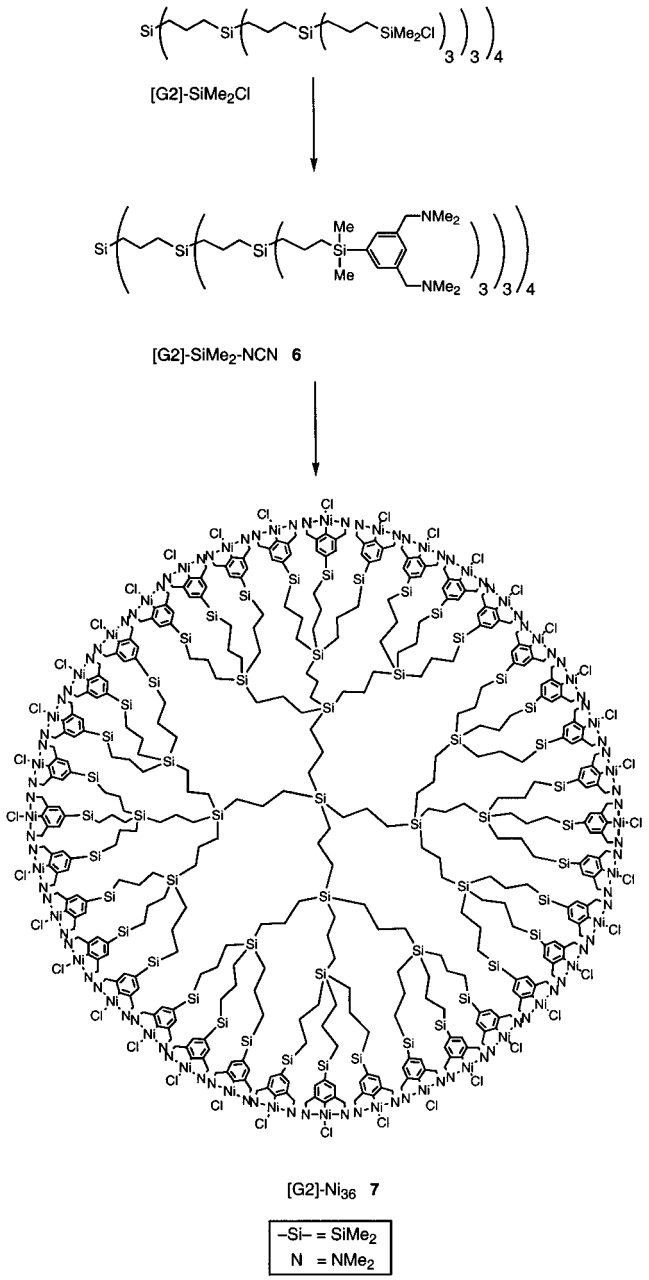

[a] *Reagents and conditions:* (i) excess Li−NCN, Et_2O, −78 °C → RT; (ii) *t*-BuLi, pentane, RT; $NiCl_2(PEt_3)_2$, Et_2O.

isotope distributions for their molecular ions (m/z = 356.2, 626.1, and 1566.2, respectively) while the most intensive peaks in these spectra were attributed to the $[M - Cl]^+$ fragment ions (m/z = 321.2, 591.1, and 1529.1, respectively). Despite the complexity of these spectra, the presence of molecular ions with correct isotopic patterns is consistent with the proposed stoichiometry of **2**−**4**. The FAB-MS spectrum of **4** shows clear isotopic patterns at m/z = 1472.3, 1437.3, 1378.4, and 1343.4 which are attributed to incomplete nickelated molecular and fragment ions [G0]-Ni_3Cl_3, [G0]-Ni_3Cl_2, [G0]-Ni_2Cl_2, and [G0]-Ni_2Cl_1, respectively. This can, obviously, be a consequence of incomplete metalation (vide supra) during the synthesis of **4**.

We applied MALDI-TOF-MS as an additional analytical tool for the relatively larger dendrimer molecules **5**−**15**. As could be expected, the mass spectrometric characterization of the larger dendrimers was hampered by the appearance of very broad peaks in the spectra of the nickelated dendrimers **5**, **7**, and **11**. This feature was partially ascribed to an incomplete nickel incorporation that gives a distribution of dendrimer species, of which the expected isotopic distributions of the molecular and fragment ions most likely strongly overlap. The broadness of these peaks may also be influenced by the oxygen-sensitivity of these nickelated dendrimers.

We were able to obtain a reasonable mass spectrum for [G2]-$SiMe_2$−NCN (**6**) (m/z = 11453, calcd 11646). The difference (193) can be explained by an acid-mediated cleavage of one NCN−H ligand precursor (calculated mass 192) ligand from the [G2] periphery and the resultant formation of a silicon cation. Also for [G1]-Ni_8 (**15**) a reasonable MALDI-TOF-MS analysis could be performed. The mass spectrum obtained for **15** clearly showed peaks at m/z = 3446.72, 3409.43, and 3349.42 which were attributed to the (incompletely nickelated) molecular and fragment ions [G1]-Ni_8Cl_8, [G1]-Ni_8Cl_7, and [G1]-Ni_7Cl_7.

The mass spectra collected for the precursor compounds and ligand systems [G1]-$SiMe_2$−$CH_2CH{=}CH_2$ (**8**), [G1]-C_3H_6−$SiMe_2$−NCN (**10**), [G1]-$(CH_2CH{=}CH_2)_8$ (**12**), and [G1]-$(NCN)_8$ (**14**) showed in all cases a clear peak for the molecular ion consistent with the proposed stoichiometry. It should be noted that for **8** and **12** a silver salt was added to increase the peak resolution, which resulted in the observation of $(M + Ag)^+$ molecular ion clusters. In the case of **10** and **14**, an acidic matrix was used to provoke the in situ formation of $(M + H)^+$ molecular ions.

Molecular Modeling of [G0]-Ni_4 (4) and [G1]-Ni_{12} (5). Molecular mechanics calculations (MM2)[19] were performed on the [G0] and [G1] nickel-containing species to give some impression about their gas-phase three-dimensional structure. The size and shape of **5** is shown in Figure 4, which represents one of the calculated conformations. For **4**, a molecular radius of ∼20 Å was calculated, while for **5** this radius was extended to ∼30 Å. It should be noted that these idealized structures may be exaggerated and *only* give information about the volume of a fully "stretched" (i.e., spherical) dendrimer. We found a profound difference between the calculated three-dimensional structures of **4** and **5**. The "front" view of **5** showed this molecule to be a generalized spherical molecule like in **4**. The "side" view (∼90° rotation) of **5**, however, showed a much more densely packed system. This phenomenon has also been reported by other authors.[20] Nevertheless, this information is useful in cases where a certain molecular size is prerequisite for the effective use of ultrafiltration techniques or membrane technology for catalyst recovery (vide infra).[7,13]

While in **4** the Ni sites are well-separated (average Ni−Ni distance ∼19 Å), in **5** these sites are situated in a much smaller volume and are in close proximity to each other (closest Ni−Ni distance about 8−11 Å). It is important to note that the nonrandom distribution of the nickel complexes in the dendrimer system **5** could have an effect on the accessibility of the Ni(II) sites in catalytic applications. In our earlier dendrimer species (see Figure 1),[6] the nickel sites were connected to the dendrimer periphery via (long) carbamate linkers, and it was anticipated that the nickel sites are well-separated as in [G0]-Ni_4 (**4**). Although we were not able to perform molecular modeling for [G2]-Ni_{36} (**7**),[21] one could imagine that in this metallodendrimer the catalytic sites are even more closely packed when compared to [G1]-Ni_{12} (**5**).

(19) CAChe Molecular Mechanics at the MM2 level, Oxford molecular group.

(20) Huck, W. T. S. Thesis Noncovalent Synthesis of Nanosize Metallodendrimers. Technical University of Twente, Twente, 1997.

(21) We were unable to perform Molecular Modeling for the [G2] derivative **7** with our software (CAChe, MM2) because of the large number of atoms present in the molecule.

Scheme 4: Synthesis of the Nickelated [G1]* Dendrimer **11**[a]

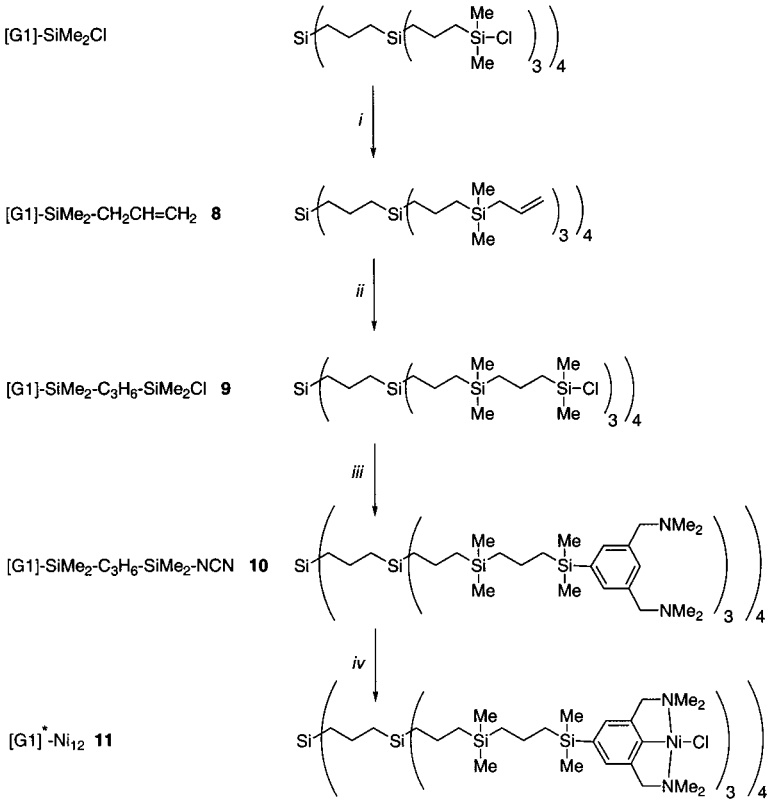

[a] *Reagents and conditions:* (i) allylmmgbr, Et_2O, RT; (ii) neat $HSiMe_2Cl$, RT; (iii) excess Li−NCN, Et_2O, −78 °C → RT; (iv) *t*-BuLi, pentane, RT; $NiCl_2(PEt_3)_2$, Et_2O.

Scheme 5: Synthesis of Nickelated [G1] Dendrimer **15**[a]

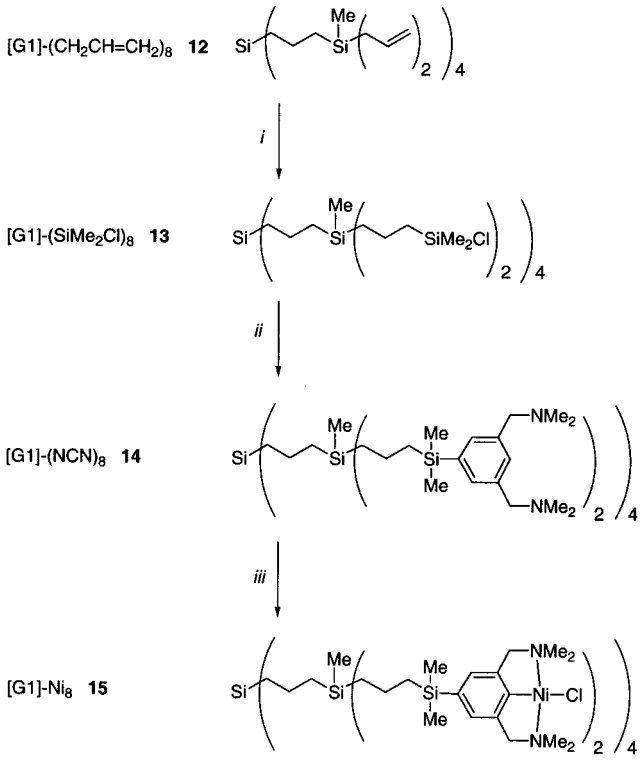

[a] *Reagents and conditions:* (i) neat $HSiMe_2Cl$, RT; (ii) excess Li−NCN, Et_2O, −78 °C → RT; (iii) *t*-BuLi, pentane, RT; $NiCl_2(PEt_3)_2$, Et_2O.

Electrochemical Studies. The redox behavior of the organonickel dendrimers in CH_3CN solution was studied by cyclic voltammetry to investigate the electronic influence of the dendrimer support on the redox potential of the peripheral [NiCl(NCN)] complexes. In principle, these metallodendrimers should yield cyclic voltammograms that correspond to the Ni(II)/Ni(III) redox couple.[8a] To keep the anion concentration constant during the oxidation process, an appropiate chloride-containing salt (viz., $[Bu_4N]Cl$) was used as supporting electrolyte. The peak potentials for the oxidation ($E_{p,a}$) and reduction ($E_{p,c}$) were measured for the model compounds **2** and **3** as well as for the dendrimer species **4**, **5**, **7**, **11**, and **15** and are collected in Table 1. It is important to emphasize that the oxidation process involved in these Ni(II)Cl complexes is a combination of an electrochemical as well a chemical reaction (EC-mechanism, note the newly formed Ni−Cl bond); that is, the transformation of a square planar Ni(II)Cl complex into a square pyrimidal $Ni(III)Cl_2$ complex. Consequently, there is no formal Nernstian relationship between the oxidative and the reductive features.[22] Nevertheless, our earlier electrochemical studies with similar organonickel(II) complexes[8a] have shown that the oxidation of the Ni(II) center is (chemically) reversible.

Interestingly, the cyclic voltammograms of all dendrimer species showed, as in the case of model compounds **2** and **3**, *single* oxidation and reduction waves consistent with *single* potentials in the oxidation and subsequent reduction of the peripheral nickel-containing complexes. This suggests that the nickel(II) sites in all dendrimer species are electrochemically independent. This is in contrast to previously reported ferrocene-derivatized carbosilane dendrimers.[23] Furthermore, the difference in oxidative and reductive peak potentials (ΔE_p) for the den-

(22) Grove, D. M.; van Koten, G.; Mul, P.; Zoet, R.; van der Linden, J. G. M.; Legters, J.; Schmitz, J. E. J.; Murrall, N. W.; Welch, A. J. *Inorg. Chem.* **1988**, *27*, 2466−2473.

(23) Cuadrado, I.; Casado, C. M.; Alonso, B.; Morán, M.; Losada, J.; Belsky, V. *J. Am. Chem. Soc.* **1997**, *119*, 7613−7614.

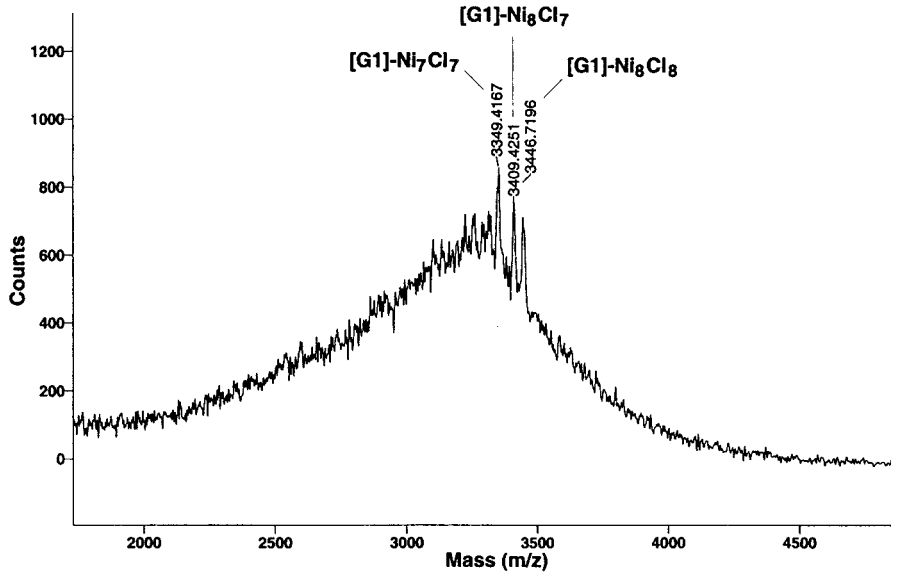

Figure 3. MALDI-TOF-MS of [G1]-Ni_8 (*15*).

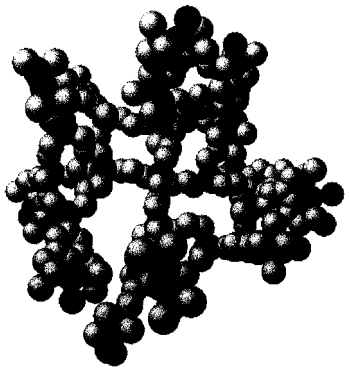

Front View of [G1]-Ni_{12} (**5**)

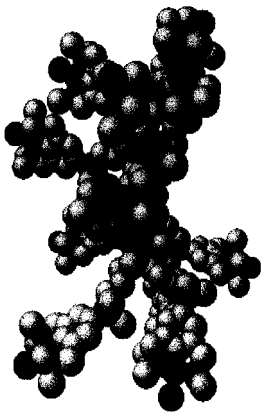

Side View (ca. 90° rotation) of [G1]-Ni_{12} (**5**)

Figure 4. Space filling model of the "front" and "side" view of the calculated structure of [G1]-Ni_{12} (**5**).

drimer species is significantly smaller than the respective difference for **2** and **3**, whereas the non-Nernstian midpoint potentials ($E_{1/2}$, see Table 1) are similar for these species. The similarity of the measured $E_{1/2}$ values points to a comparable electronic influence of the dendritic support and the $SiMe_3$ group on the nickel center in the dendrimer species and the model compound **2**, respectively.

Table 1. Cyclic Voltammetry Results of the Model Compounds **2** and **3** and the Nickelated Dendrimers in CH_3CN[a,b]

compound	$E_{p,a}$/V	$E_{p,c}$/V	ΔE_p/V	$E_{1/2}$/V[c]
2	−0.103	−0.595	0.492	−0.33
3	−0.172	−0.526	0.354	−0.34
4, [G0]-Ni_4	−0.208	−0.435	0.227	−0.32
5, [G1]-Ni_{12}	−0.278	−0.413	0.135	−0.35
7, [G2]-Ni_{36}	−0.276	−0.412	0.137	−0.34
11, [G1]′-Ni_{12}	−0.273	−0.414	0.141	−0.34
15, [G1]-Ni_8	−0.298	−0.397	0.099	−0.34

[a] For conditions see Experimental Section. [b] Peak potentials are given against the Fc/Fc^+ couple in the same solvent. [c] Non-Nernstian midpoint potential defined as $E_{1/2} = {}^1/_2(E_{p,a} + E_{p,c})$.

Catalysis with the Nickelated Dendrimers. In comparative studies, the arylnickel complexes of general formula [NiX-($C_6H_2\{CH_2NMe_2\}_2$-2,6-R-4)] showed to be efficient catalysts in atom-transfer radical addition (ATRA) chemistry (i.e., polyhalogenated alkane addition to olefins, the Kharasch addition reaction).[8] In addition, we recently prepared catalytically active nickelated carbosilane dendrimers[6] with activities per nickel atom comparable to those observed for their mononuclear analogues. We therefore investigated the activity of the novel nickelated dendrimers (vide supra) in the ATRA reaction using methyl methacrylate (MMA) as substrate and carbon tetrachloride (CCl_4) as the polyhalogenated alkane. The same conditions were used as reported in our previous studies on this type of catalysis.[6,8] The results obtained for the nickelated dendrimers were compared with the parent model [NiCl($C_6H_2\{CH_2NMe_2\}_2$-3,5-($SiMe_3$)-4] (**2**) and di-nickelated $Me_2Si[C_6H_2\{CH_2NMe_2\}_2$-3,5-(NiCl)-4]$_2$ (**3**). The catalytic data are collected in Table 2 and visualized in Figures 5 and 6.

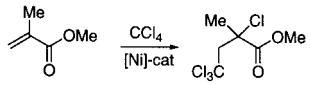

The total turnover number (TTN) after 4 h, calculated for the mono-nickel complex **2** was in the same range as that found for similar [NiX(NCN)] complexes, which were applied in the same catalytic reaction. The initial reaction rate for **2** reflected in turnovers per h, however, was approximately 30% lower than that measured for [NiBr($C_6H_3\{CH_2NMe_2\}_2$-2,6)], the model compound used as a standard in our earlier work in this area.[6]

Table 2. Catalytic and Kinetic Data for the ATRA Reaction of CCl_4 to MMA Using the Model Compounds **2** and **3** and the Nickelated Dendritic Catalysts[a]

compound	time (h)	conversion[b] (%)	TOF (per Ni per h)[c]	TTN (per Ni)
2	0.25	15	163	277[e]
	2	91		
3	0.25	9	108	311[e]
	2	74		
4, [G0]-Ni_4	0.25	9	111[d]	324[d,e]
	2	79		
5, [G1]-Ni_{12}	0.25	3	44[d]	63[d,e]
	2	17		
7, [G2]-Ni_{36}	0.25	0.2	3[d]	11[d,e]
	2	1.0		
11, [G1]*-Ni_{12}	0.25	8	102[d]	310[d,f]
	2	54		
15, [G1]-Ni_8	0.25	5	53[d]	284[d,f]
	2	27		

[a] In all catalytic runs (duplo experiments) the concentration of nickel was kept constant at $\sim 9 \times 10^{-5}$ mol. [b] Selectivity for the formation of the 1:1 adduct of methyl methacrylate and CCl_4 is >99%. Conversion calculated from the formation of the 1:1 addition product as determined with GC analysis using dodecane as an internal standard. [c] During the first 15 min. [d] Values corrected for nickel incorporation using the NMR spectroscopic and elemental analyses data. [e] After 4 h. [f] After ~22 h.

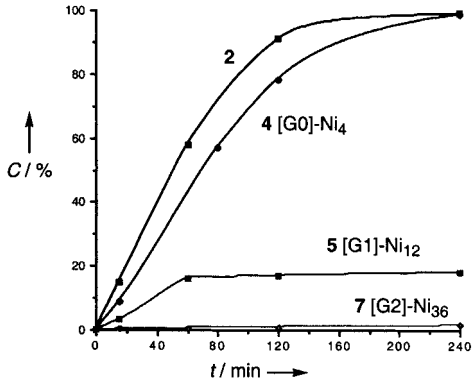

Figure 5. Visualization of the catalytic results obtained for nickelated compounds **2**, **4**, **5**, and **7**. Abbreviations used: C = conversion, t = time. The curve corresponding to the catalytic performance of **3** has been omitted for clarity reasons.

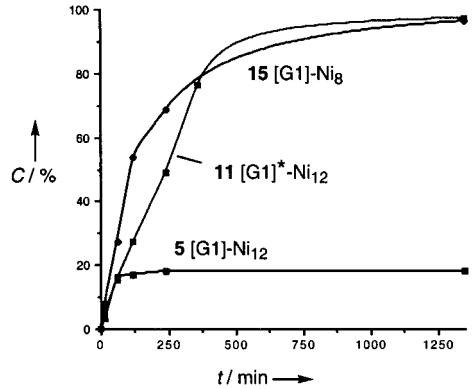

Figure 6. Visualization of the catalytic results obtained for nickelated compounds **5**, **11**, and **15**. Abbreviations used: C = conversion, t = time.

This lower initial activity was attributed to the presence of a Ni−Cl bond in **2** (cf., Ni−Br bond in [Ni(NCN)Br]). As there is a fast exchange of the bromide for a chloride anion in the unsubstituted complex [Ni(NCN)Br] in the presence of a large excess of CCl_4 during catalysis,[8a,b] it is eventually the *para* substituent R (Figure 2) that has the greatest influence on the catalytic activity. This latter effect has been studied and reported elsewhere.[8a] The halide influence on the initial reaction rate is known to decrease in the order I ≈ Br > Cl.[8a]

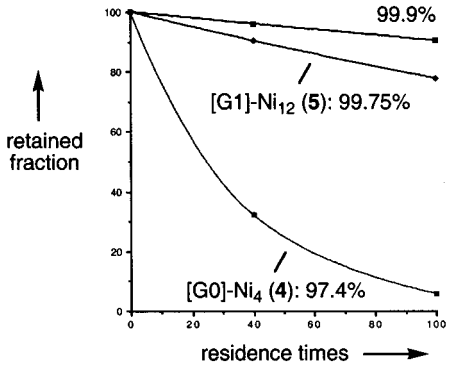

Figure 7. Display of the retained fractions of [G0]-Ni_4 (**4**) and [G1]-Ni_{12} (**5**) in a membrane reactor.[26]

The decrease in catalytic activity found for **4** compared to **2** in terms of the initial reaction rate (i.e., TOF/h during the first 15 min, Table 2) is ~30% which is in line with our earlier results in this area.[6] For [G1]-Ni_{12} (**5**) however, a dramatic drop of ~70% in initial catalytic activity per nickel atom was observed together with the precipitation of an *insoluble* purple/brown solid (**P-5**) after ~1 h. The large difference in (initial) activity and TTN/Ni site between **5** and the model derivatives **2** and **3** could not be explained by the fact that **5** is not fully metalated. Additionally, for [G2]-Ni_{36} (**7**) almost no catalytic activity (conversion <1.5% after 4 h) was observed. Furthermore, after ~3 h, again an *insoluble* purplish solid (**P-7**) precipitated which did not exhibit any catalytic activity (Figure 5).

The two alternative [G1] nickelated carbosilane dendrimers [G1]*-Ni_{12} (**11**) and [G1]-Ni_8 (**15**) were also applied in the same standard ATRA reaction (Figure 6 and Table 2). A marked difference was observed when the catalytic activity of **5** was compared with the extended analogue [G1]*-Ni_{12} (**11**). First, the conversion of MMA into the addition product after 4 h was already 49% (cf., the *maximum* conversion of ~20% in the case of **5**) and became almost quantitative (97%) after 22 h when **11** was used as catalyst. A second major difference is that the precipitation of a purple solid did not occur until all MMA had been converted into product. This latter phenomenon was monitored in time, and after 6 h, still no observable precipitation had occurred. It must be emphasized that the initial reaction rates per nickel site in **11** and **4** were comparable. The TTN for **11** (310) was comparable with those obtained in the catalytic reactions employing the model derivative **2** or **4** with TTNs of 277 and 324, respectively. The use of the nickelated dendrimer [G1]-Ni_8 (**15**) (TTN = 284) gave results similar to those of [G0]-Ni_4 (**4**) and [G1]*-Ni_{12} (**11**), with (only) a slightly reduced initial reaction rate (Table 2).

Membrane Catalysis with [G0]-Ni_4 (4) and [G1]-Ni_{12} (5). Dendrimers **4** and **5** were also tested for their degree of retention (Figure 7)[24] and catalytic characteristics (Figure 8) in a membrane reactor equipped with a SelRO-MPF-50 nanofiltration membrane.[25] Although the measured retention in this membrane system was neither quantitative for **4** (97.4%) nor for **5** (99.75%), theoretical calculations (Figure 7) showed that **5**

(24) The degree of retention for [G0]-Ni_4 (**4**) and [G1]-Ni_{12} (**5**) in CH_2Cl_2 at 25 °C using the SelRO-MPF-50 membrane was measured by photometric measurements taking into account both the nickel concentration in the retained fraction and in the "leached" fraction.

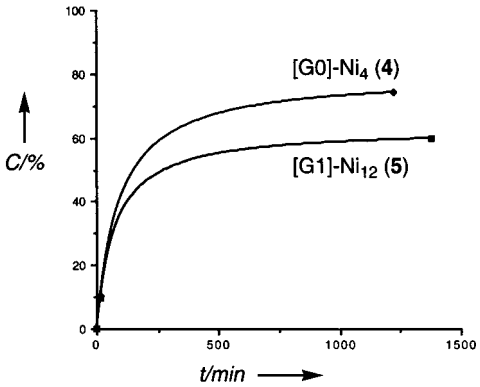

Figure 8. Display of the membrane catalysis with **4** and **5**. Abbreviations used: C = conversion, t = time.[26]

Table 3. Membrane Catalysis Results Obtained for **4** and **5**[a]

compound	time (h)	conversion (%)	TOF (per Ni per h)	TTN (per Ni)
4, [G0]-Ni_4	0.25	11	98[c]	
	20.4	74		173[c]
5, [G1]-Ni_{12}	0.25	9.8	88[c]	
	23	60		154[c]
5, [G1]-Ni_{12}[b]	0.25	7	88[c]	
	91.4	45		148[c]

[a] See Table 2 for details of this catalysis. [b] In the presence of a large excess of [NBu4]Br. [c] Values corrected for nickel incorporation using the NMR spectroscopic and elemental analyses data.

should be sufficiently large enough for the use in a continuous operating reactor without significant leaching of the catalyst after 100 cycles.[26] The leaching of the catalytic species not only will depend on the membrane perfection and permeability, but also on the chemical stability of the catalyst system. It is therefore important to note that the carbon-metal bond (i.e., Ni−C_{aryl}) and the connecting dendrimer-ligand Si−C bonds in **4** and **5** are not easily cleaved under the reaction conditions.

During the catalytic membrane experiments in the presence of **4** or **5**, the precipitation of *insoluble* purple species (**P-4** and **P-5**) after 40 min. was again noted. However, in contrast to the standard batch reaction carried out with [G1]-Ni_{12} (**5**), **P-5** still showed significant catalytic activity in the Kharasch reaction, and in the case of **P-4**, conversion of MMA into the adduct was achieved up to 74% after ∼20 h (Table 3, Figure 8). The addition of a large excess of [Bu_4N]Br did, however, prevent the formation of **P-5** in the case of **5** (Table 3), but as a result, part of the addition product contained both chlorine *and* bromine atoms.[27] Another effect from the addition of [Bu_4N]Br is a lower activity (after 15 min) when compared to the reaction without this additive. After ∼90 h, the conversion reached only 45% in the presence of **5** as catalyst. These latter results significantly differed from those obtained for **5** in the batch reaction (Table 2) and pointed to a slower deactivation process. We therefore attempted to use [G1]-Ni_{12} (**5**) in a continuous operating membrane reactor system equipped with a SelRO-MPF-50 membrane

(25) A SelRO-MPF-50 membrane was used and this membrane consists of polyphenylen- oxide-, polysulfonated-, and haloalkylated polyphenelenoxide-based materials. This membrane is hydrophobic and can retain opportunistic H_2O. The reactor material was made from poly(propylene).

(26) A cycle or residence time is defined as the time needed to fully replace one membrane reactor volume.

(27) This has also been observed in crossover experiments with [NiBr(NCN)] in the presence of MMA and a mixture of CCl_4/CBr_4. The experiments revealed the formation of eight products (all 1:1 adducts). This has been ascribed to a statistical incorporation of both bromide as well as chloride into the products through the initial formation of an "inner- sphere" intermediate.[9] The [NBu_4]Br additive is thought to be involved in a halide methathesis reaction with the initially formed Ni(III)Cl_2 intermediate.

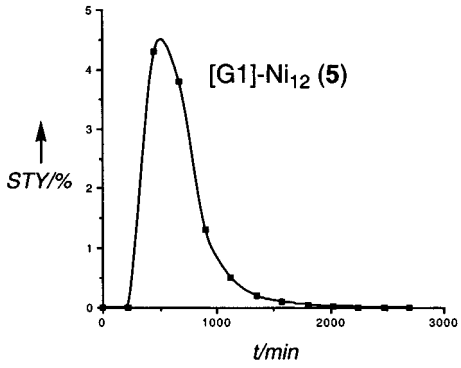

Figure 9. Continuous membrane catalysis carried out with **5**. Abbreviations used: STY = space time yield, t = time.

(Figure 9) with a continuous feed of [Bu_4N]Br to prevent catalyst precipitation.

Despite the fact that **5** was successfully retained in the reactor and that a precipitation of **5** was avoided, a fast decrease of the conversion per time unit (after 33 h ≈ 0) was observed with a low TTN/Ni of only 20. After the continuous membrane reaction (i.e., after the reactor volume was replaced 64 times), both the retained fraction as well as the leached fraction were subjected to ICP mass spectrometric analysis in order to calculate the amount of nickel present. From these data, the degree of retention for **5** in the continuous operating membrane reactor system was determined at 98.6%, which closely resembled the measured retention found for **5** (99.8%, vide supra) in a batch reactor. Although a retention of 98.6% theoretically leads to loss of catalytic material relatively quickly inside the continuous membrane reactor, it cannot solely explain the observed fast deactivation of [G1]-Ni_{12} (**5**) in the reactor.

Mechanistic Arguments. In the ATRA (i.e., Kharasch) reaction of CCl_4 to MMA, the addition of a nickel catalyst to a mixture containing these substrates is accompanied by an immediate color change, giving rise to purple/brown solutions. For the model catalysts **2** and **3** and dendrimer species **4**, **11**, and **15**, purple precipitates started to form after the conversion of MMA were virtually *complete*. In contrast to this observation, when **5** or **7** were used as catalyst in this system, the precipitation of an *insoluble* purple solid and a total deactivation of the catalytic system was already noticed after approximately 1 and 3 h, respectively, while conversion of MMA to the 1:1 addition product of only 18 and 1.5%, respectively, was achieved. Similar observations of the formation of insoluble purple species *during* catalysis were made in the membrane experiments carried out with **4** and **5**.

Interestingly, comparable observations were performed for *polymer*-bound [Ni(NCN)Br] complexes applied in ATRA chemistry.[28] Spectroscopic studies (ESR, FT-IR, and UV/Vis) indicated that the purple compound in this case was a material containing paramagnetic Ni(III) centers. Furthermore, the catalytic activity of these polymer catalysts was strongly dependent on the nickel catalyst loading. For the polymeric catalytic materials with a relatively low loading of nickel catalyst (cf., [G0]-Ni_4 (**4**)), the precipitation of a purple/brown solid during catalysis did not appreciably lower the activity of the immobilized Ni(II) complexes. A high increase in nickel loading in the same polymer system (cf., [G1]-Ni_{12} (**5**) and [G2]-Ni_{12} (**7**)) led to a significantly lower catalytic activity per nickel atom (∼60%) attributed to a decrease in *initial* solubility of the catalytic species. The latter feature was held responsible for the

(28) van de Kuil, L. A.; Grove, D. M.; Zwikker, J. W.; Jenneskens, L. W.; Drenth, W.; van Koten, G. *Chem. Mater.* **1994**, *6*, 1675.

Scheme 6: Postulated Key Intermediate Steps in the ATRA (i.e., Kharasch) Reaction Catalyzed by [NiCl(NCN)] Complexes[a]

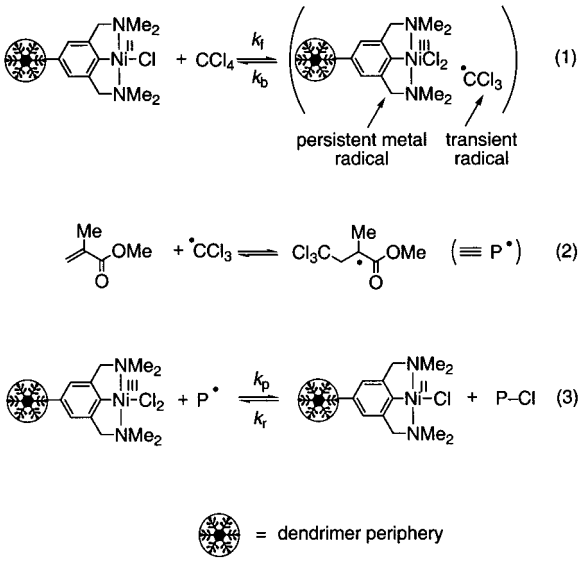

[a] Abbreviations used: k_f = forward reaction, k_b = back reaction, k_p = forward product-forming reaction, k_r = back "radical-reforming" reaction.

formation of a relatively inactive, "heterogeneous" reaction mixture. The reduced solubility characteristics found for **5** and **7** under standard homogeneous conditions and the (total) deactivation of these catalysts are in line with these former results.

The purple color observed in this type of ATRA reaction catalyzed by [NiX(NCN)] complexes was associated with the formation of a relatively stable, intermediate species in the postulated catalytic cycle (Scheme 6).[9] In the first step of this cycle, the nickel(II) complex reacts with a polyhalogenated alkane, in this case CCl_4, to give a nickel(III) intermediate (i.e., a persistent radical, vide infra) and a CCl_3 transient radical (see eq 1, Scheme 6). The latter stays fixed in the coordination sphere of the Ni(III) center.[29] In a subsequent step (eq 2), the CCl_3 radical reacts with the olefinic substrate to yield a product radical P•, which in the last step (eq 3) is converted into a perhalogenated product by an atom-transfer "back" reaction from the persistent radical (i.e., the Ni(III) complex) to regenerate the catalytically active Ni(II) species. Although this type of catalysis involves highly reactive transient radical species, the *selectivity* for the ATRA reaction catalyzed by [NiX(NCN)] complexes is virtually quantitative when CCl_4 is used in a large excess.[30]

The observed selectivity behavior can be explained by the persistent radical effect, that was recently formulated and reviewed by Fischer.[31] At the same time, Matyjaszewski[32] used the concept of the persistent radical effect to describe the fundamental steps in the ATRA (i.e., Kharasch) reaction catalyzed by metal halide complexes. Similar mechanistic steps are also postulated in Scheme 6. The abstraction of a halide atom from CCl_4 and the concomitant inner-sphere oxidation of the Ni(II) complex produces a persistent radical that does not self-terminate or propagate (*i.e.*, the newly formed Ni−Cl bond is not activated). The transient CCl_3 radical, however, is involved in both termination as well as addition reactions. In general, the highly reactive character of this transient radical leads to a very low steady-state concentration of radicals, and thus the contribution of termination is, therefore, negligible. Another important aspect is that the polyhalogenated substrate should generate radicals more easily than the (final) products and should only give monoaddition. It was found that the catalytic system MMA/CCl_4/[NiX($C_6H_2\{CH_2NMe_2\}_2$-3,5-R-4)] (Figure 2) indeed obeys all of these characteristics put forward by the persistent radical concept, and this makes it possible to give an explanation for the (membrane) catalysis results and the observed precipitation of purple solids during catalysis (vide infra).

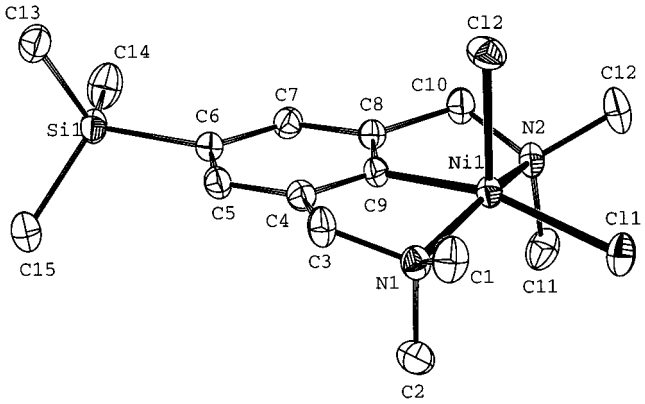

Figure 10. Displacement ellipsoid plot (ORTEP, 50% probability level) of the molecular structure of **16**. Selected bond lengths (Å) and angles (deg) with esd's in parentheses: Ni−Cl1 2.2761(5), Ni−Cl2 2.2756(6), Ni−C9 1.8850(16), Ni−N1 2.0324(14), Ni−N2 2.0283(14), Cl1−Ni−C9 164.01(6), N1−Ni−N2 154.05(6), N1−Ni−C9 82.46-(6), Cl1−Ni−N1 93.44(4), Cl2−Ni−N1 100.34(4).

Identification of the Purple Species. To identify the *insoluble* purple species that precipitated during catalysis under the standard batch conditions, we performed a model studies with the mononuclear model [NiCl($C_6H_2\{CH_2NMe_2\}_2$-2,6-$SiMe_3$-4)] (**2**). Thus, the organonickel(II) complex **2** was treated with an excess of CCl_4 in the absence of MMA (eq 2).

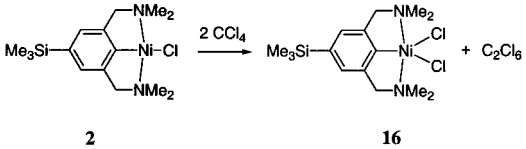

2 **16**

This reaction was carried out to mimick the termination of ATRA catalysis by [NiX(NCN)] complexes (i.e., when [MMA] $\approx$ 0). The addition of CCl_4 to **2** leads immediately to a dark purple to brown solution. After workup and crystallization of the product, dark red to brown crystals were obtained, which were analyzed by microanalyses and pointed to the formation of the corresponding Ni(III) dichloride species [$NiCl_2$($C_6H_2\{CH_2NMe_2\}_2$-2,6-$SiMe_3$-4)] (**16**). To unambiguously establish the structure of the product, an X-ray crystal structure determination was carried out. The molecular structure of **16** is depicted in Figure 10 (see the Supporting Information for further details). Figure 10 shows that the geometry around the formal Ni(III)

(29) When a mixture of CBr_4/CCl_4 and [NiBr(NCN)] is analyzed with GLC/GC−MS, three organic products were identified as $CBrCl_3$, CBr_2Cl_2, and CBr_3Cl. This corroborates the view that the initial process comprises the formation of an inner-sphere activated complex derived from the nickel complex and the polyhalogenated alkane.

(30) Under the ATRA conditions employed (i.e., a high polyhalogenated alkane/Ni catalysts ratio) there is exclusive formation of the 1:1 adduct. However, at a low concentration of this polyhalogenated alkane, controlled radical polymerization of MMA can be carried out with this type of nickel complexes. See: Granel, C.; Dubois, Ph.; Jérôme, R.; Teyssié, Ph. *Macromolecules* **1996**, *29*, 8576.

(31) Fischer, H. *J. Polym. Sci., Part A: Polym. Chem.* **1999**, *37*, 1885 and references therein.

(32) (a) Matyjaszewski, K., Ed. *Controlled Radical Polymerization*; ACS Symposium Series 685, American Chemical Society, Washington, DC, 1998. (b) Matyjaszewski, K. *Chem. Eur. J.* **1999**, *5*, 3095 and references therein.

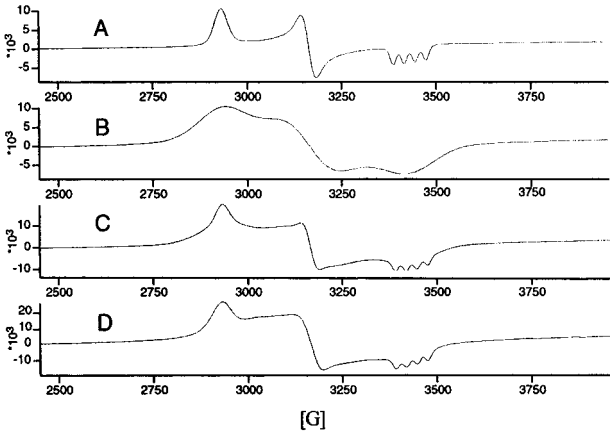

Figure 11. ESR spectra recorded for the nickel(III) complex **16** and the precipitate **P-5** derived from [G1]-Ni_{12} (**5**).

center is best described as square pyramidal with the nickel atom displaced from the basal plane. No unusual bond distances and bond angles were found for **16** when compared to a related organonickel(III) diiodide complex.[33]

We further investigated the formation of **16** by analysis of the organic products (GC−MS) when **2** was exposed to an excess of CCl_4 in the absence of MMA. From the mass spectra it became clear that two major organic products were obtained depending on the presence of a cosolvent (i.e., CH_2Cl_2). In the presence of CH_2Cl_2, two products were identified with fragment ions that displayed peaks at $m/z = 201$ and 215. The former peak could easily be assigned to the fragment ion $C_2Cl_5^+$ while the latter peak could be ascribed to a fragment ion with a molecular formula $C_3H_2Cl_5^+$. The presence of characteristic isotope patterns due to the presence of multiple chloride atoms in both ions suggested the formation of the perhalogenated alkane compounds C_2Cl_6 and $C_3H_2Cl_6$. The structure of the latter compound was not elucidated. It should be noted that in the absence of CH_2Cl_2, only the formation of C_2Cl_6 was observed (eq 2).[34]

The purple precipitate **P-5** obtained from the dendrimer catalyst **5** using the standard catalytic protocol was also isolated and a mass balance of ~80% was calculated taken into account a full conversion of the Ni(II)Cl into Ni(III)Cl_2 sites in **5**. The purple precipitate **P-5** and the model derivative [$NiCl_2$(C_6H_2\{CH_2NMe_2\}$_2$-2,6-$SiMe_3$-4)] (**16**) were analyzed by means of ESR spectroscopy (vide infra).

ESR Spectroscopy of P-5 and 16. Due to the insolubility of the purple/brown precipitate **P-5** in all the common organic solvents and H_2O, we used solid-state ESR spectroscopy for an analysis. The ESR spectrum obtained for **P-5** (Figure 11D) was compared to the spectrum obtained for the parent Ni(III) compound [$NiCl_2$(C_6H_2\{CH_2NMe_2\}$_2$-2,6-$SiMe_3$-4)] (**16**) in toluene glass at 120 K (Figure 11A).

The solid-state ESR spectrum of **P-5** largely resembles the ESR spectrum of **16**, and the former is regarded as a superposition of independent spectra for different Ni(III) complexes. Theoretical modeling showed that spectrum D most probably consists of two phases. In one phase, the nickel(III) sites are more closely packed, leading to a faster relaxation mode and give rise to a signal with a relative high dipolar broadening (Figure 11B). In the other phase, the Ni(III) sites are more separated and this "spectrum" is comparable to the ESR spectrum of **16** (Figure 11A) measured at low temperature. Combination of the latter two spectra yielded the theoretical spectrum C, which is similar to the measured ESR spectrum for **P-5** (Figure 11D).[35]

Two stoichiometric mixtures of [$Ni^{II}Cl$(C_6H_2\{CH_2NMe_2\}$_2$-2,6-$SiMe_3$-4)] (**2**) and [$Ni^{III}Cl_2$(C_6H_2\{CH_2NMe_2\}$_2$-2,6-$SiMe_3$-4)] (**16**), and **2** and [$Ni^{III}Br_2$(NCN)] (i.e., Ni(II)/Ni(III) mixed valence complex mixtures) were also subjected to ESR spectroscopic investigations in toluene glass at ~120 K. The ESR spectra obtained for both mixtures were identical to the ESR spectra of the single Ni(III)X_2 (X = Cl or Br) species gathered under the same conditions and no clear evidence was found for a significant intermolecular interaction between the Ni(II) and Ni(III) complexes under these experimental conditions.

Mode of Deactivation. In the absence of olefinic substrate (i.e., when [MMA] = 0), the Ni(III) derivative [$NiCl_2$(C_6H_2\{CH_2NMe_2\}$_2$-2,6-$SiMe_3$-4)] (**16**) is produced by a process that probably involves a C−Cl bond activation of CCl_4 by the Ni(II) complex **2** (eq 2). The formation of C_2Cl_6 is obvious evidence for this and is ascribed to the termination reaction of two CCl_3 radicals. For each C_2Cl_6 molecule formed in this way, 2 equiv of the persistent radical **16** remain which in this case cannot be recycled into the Ni(II) complex. To no surprise, in the presence of a cosolvent, another organic product (i.e., $C_3H_2Cl_6$) is formed. The formation of the latter is likely a result of a reaction of the transient radical CCl_3 with the chlorinated solvent. This suggests that the transient radical is involved in outer-sphere reactions, and, furthermore, that the reaction behavior of the transient radical is no longer controlled by the persistent radical (i.e., **16**).

Molecular modeling performed on **5** indicated that the Ni sites in this dendrimer are in much closer proximity when compared to **4** and the nickelated [G1] dendrimer described earlier (Figure 1).[6] In this regard, it should be noted that in these dendrimer species the [NiCl(NCN)] catalytic sites are *nonrandomly* distributed. During catalysis, this latter feature may lead to proximity effects such as termination (via coupling as observed in the synthesis of the Ni(III) complex **16**) of radical intermediates or electron-transfer processes within the dendrimer molecule itself. Obviously, these (kinetically based) deactivation processes will likely depend on the spatial separation (or proximity effect) of the Ni(II) catalytic sites. This was supported by the use of the two alternative [G1] dendrimer catalysts [G1]*-Ni_{12} (**11**) and [G1]-Ni_8 (**15**), in which the Ni(II) sites are more separated from each other as compared to [G1]-Ni_{12} (**5**) and [G2]-Ni_{36} (**7**). These data supported the view that the effectiveness of the back reaction between the peripheral Ni(III) persistent radical and the product radical P$^\bullet$ (Scheme 6) follows the series **7** < **5** < **2**. Ultimately, outer-sphere reactions of the transient radical species CCl_3 as described in the preparation of **16** would give rise to *irreversible* formation of *catalytically inactive* Ni(III) complexes on the periphery of the dendrimer. The formation of abundant Ni(III) sites on the periphery of the dendrimer was confirmed for the precipitate **P-5** obtained from dendrimer **5**. The solid-state ESR spectrum of **P-5** clearly showed a large resemblance with the ESR spectrum recorded

(33) Grove, D. M.; van Koten, G.; Zoet, R.; Murall, N. W.; Welch, A. *J. Am. Chem. Soc.* **1983**, *105*, 1379.

(34) The *quantitative* analysis of the formation of C_2Cl_6 by treatment of the nickelated derivative with CCl_4 was hampered because of the insoluble character of the nickel complex in this solvent. The same accounts for the dendrimer species. In the presence of a co-solvent, another product with unknown structure (probably $C_3H_2Cl_6$) was found as mentioned in the main text.

(35) We attempted a spin quantification in **P-5** using **16** and a $CuSO_4$ sample as standards. The results indicated a (low) conversion of 13% of the present Ni(II) into Ni(III) sites. However, due to the nonrandom distribution of the Ni(II) sites in **P-5** compared to **16**, this figure may be speculative. As for **16**, the same *g*-values were found for **P-5** with an increased line-broadening.

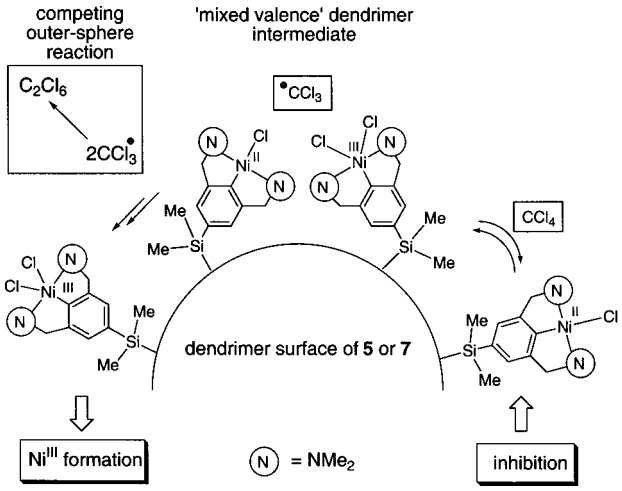

Figure 12. Schematic deactivation mode for dendrimer catalysts [G1]-Ni_{12} (**5**) and [G2]-Ni_{36} (**7**).

for the mononuclear model [$NiCl_2(C_6H_2\{CH_2NMe_2\}_2$-2,6-$SiMe_3$-4)] (**16**). In general, the Ni(III)X(NCN) complexes are *less* soluble in the common organic solvents compared to their respective Ni(II) derivatives. Therefore, the observation of purple precipitates during these catalytic reactions with **5** and **7** further supported the proposed formation of polynickel(III) dendrimers. This mode of deactivation of **5** and **7** is schematically visualized in Figure 12 and is based on all the presented results and mechanistic arguments (vide supra).

A distinct difference between the batch reactions and the membrane experiments was found for the catalytic activity of the purple precipitates **P-4** and **P-5**. Whereas for **5** a total deactivation was observed under the batch conditions, the purple precipitate **P-5** in the membrane reactor showed better catalytic activity and significantly higher substrate conversion (Tables 2 and 3), although the reaction rate was relatively low. It is possible that the radical intermediates involved in this ATRA reaction (Scheme 6) interacted with groups present in the polymeric material of the membrane.[36] Consequently, the irreversible formation of Ni(III) sites in the dendrimer catalyst **5** was slowed down. The addition of [NBu_4]Br prevented the precipitation of the catalytic species on the membrane surface during catalysis. The perhalogenated products contained, as a result, some bromine atoms. This indicates that the addition of halide could compete with the presumed interaction of the catalytic species with the membrane surface. As a logical consequence of the addition of an excess of [NBu_4]Br the catalytic activity was relatively lowered (Scheme 6). Nevertheless, the membrane catalysis results obtained with **4** and **5** helped to establish that recycling of these dendrimers is possible. This work also demonstrates that the compatibility between the membrane system and the type of catalysis is an important parameter that, at least in this case, needs to be studied in more detail and optimized before an efficient continuous catalysis operation can be carried out. Therefore, the development of other nanofiltration membranes which can stand long-term exposure to (chlorinated) organic solvents will play a crucial role.

(36) A *deactivation* of the catalytic species by interaction with either the membrane material or the reactor material[26] can be ruled out. This has been investigated by separate experiments in which the influence of the membrane material or reactor material has been studied separately. However, a *positive* influence on the catalytic activity of [G0]-Ni_4 (**4**) and [G1]-Ni_{12} (**5**) by such interactions is possible leading to a slower deactivation process (i.e., Ni(III) formation).

(37) Although we have done several attempts to obtain reliable analytical (C, H, N) data for **11** and **15**, in each case the measured analyses were significantly lower than expected. The relative ratios, however, do correspond to the expected relative ratios and point the proposed ligand-to-metal combination.

Conclusions

In summary, we have detailed a new and simple synthetic methodology for the production of metal-centered carbosilane dendrimers by using polylithiated precursors. These new metallodendrimers were successfully employed as homogeneous catalysts in the ATRA (i.e., Kharasch) reaction. The use of ultrafiltration membrane technology as a tool for the separation of macromolecular catalysts from the product stream was demonstrated. The size properties of [G1]-Ni_{12} (**5**) (~25−30 Å diameter) allowed the catalysis to be operated under continuous conditions with retention of the catalyst in the membrane reactor and with no significant loss of catalytic material. However, the formation of a purple precipitate, which contains Ni(III) sites, was a limiting factor. From this work it became clear that there exists a "proximity effect" between the peripheral Ni(II) sites in [G1]-Ni_{12} (**5**) and [G2]-Ni_{36} (**7**), which translates into lower catalytic efficiencies and irreversible formation of inactive Ni(III) sites. Our future work will be focused on this aspect and we are currently investigating the synthesis and application of other types of dendrimer catalysts.

Experimental Section

General. All sensitive, organometallic manipulations were performed under a dry and deoxygenated dinitrogen atmosphere using standard Schlenk techniques unless otherwise stated. All solvents were carefully dried and distilled prior to use. The reagents that were purchased commercially were used without further purification. The nanofiltration membrane SelRO-MPF-50 was obtained from Koch International GmbH, Düsseldorf, Germany. The starting materials [G1]-$SiMe_2Cl$,[4a] [G2]-$SiMe_2Cl$,[4a] [G1]-$(CH_2{-}CH{=}CH_2)_8$,[4] [G0]-$SiMe_2{-}NCN$,[12a] [G1]-$SiMe_2{-}NCN$,[11a] 1-bromo-3,5-bis[(dimethylamino)methyl]benzene,[14] and 1-trimethylsilyl-3,5-bis[(dimethylamino)-methyl]benzene[14] were prepared according to literature procedures. ^1H, $^{13}C\{^1H\}$, and $^{29}Si\{^1H\}$ NMR spectra were recorded on a Bruker AC200/AC300 or Varian Inova/Mercury 200 or 300 MHz spectrometer. Chemical shifts are given in ppm using TMS as an external standard. Coupling constants are given in Hertz (Hz). FAB-MS spectra were obtained from the Analytical Chemistry Department of the Utrecht University. Photometric measurements were carried out with a Shimadzu UV160 A, CPS-240 A apparatus. ESR spectra were obtained from the Department of Molecular Spectroscopy of University of Nijmegen. Elemental analyses were performed by Dornis und Kolbe, Mikroanalytisches Laboratorium, Mülheim a.d. Ruhr, Germany. Please note that a full description of the experimental procedures and analytical data of compounds **1**−**5** and **8**−**15** have been deposited as Supporting Information. The procedures described here for compounds **6** and **7** may be regarded as examples for the other model/dendrimer compounds.

[G2]-$SiMe_2$-NCN (6). This compound was prepared in a similar way as has been described for [G0]-$SiMe_2{-}NCN$ and [G1]-$SiMe_2{-}NCN$.[11a] To a solution of 1-bromo-3,5-bis[(dimethylamino)methyl]benzene (3.04 g, 11.2 mmol) in Et_2O (30 mL) was added *t*-BuLi (11 mL of a 1.7 M solution in pentane, 18.7 mmol) at −78 °C and the resultant white suspension stirred for 20 min, whereupon [G2]-$SiMe_2Cl$ (1.21 g, 0.201 mmol) in Et_2O (25 mL) was added. After isolation and purification, a extremely viscous oil was obtained (1.13 g, 0.097 mmol, 48%). ^1H NMR (C_6H_6): δ = 7.63 (s, 72H, Ar−H), 7.58 (s, 36H, Ar−H), 3.46 (s, 144H, CH_2N), 2.22 (s, 432H, $N(CH_3)_2$), 1.69 (br, $SiCH_2CH_2-$), 1.07 (br, $-CH_2SiMe_2-$), 0.87 (br, $SiCH_2CH_2-$), 0.45 (s, 216H, $Si(CH_3)_2$). $^{13}C\{^1H\}$ NMR (C_6H_6): δ = 139.3, 139.0, 133.1, 130.6 (Ar−C), 64.7 (CH_2N), 45.6 ($N(CH_3)_2$), 21.2, 19.3, 17.9 (3 × CH_2), −2.2 ($Si(CH_3)_2$). $^{29}Si\{^1H\}$ NMR (C_6D_6): δ = 1.48, 1.14, 0.75 (inner + outer *Si*), −3.76 (*Si*-aryl). MALDI-TOF-MS: *m*/*z* 11453 $(M - NCN)^+$. Calcd *m*/*z* 11454. Anal. Calcd for $C_{660}H_{1212}N_{72}Si_{53}$: C 68.07, H 10.49, N 8.66, Si 12.78. Found: C 68.17, H 10.38, N 8.61, Si 12.70%.

[G2]-Ni_{36} (7). To a solution of **6** (0.29 g, 0.025 mmol) in pentane (40 mL) was added *t*-BuLi (2.4 mL of a 1.7 M solution in pentane, 4.0 mmol). The resultant red suspension was stirred for 1 h and the excess *t*-BuLi removed by decantation of the pentane layer. Then a solution of $NiCl_2(PEt_3)_2$ (0.61 g, 1.67 mmol) in Et_2O (40 mL) was added and the obtained orange to red suspension stirred for 17 h. Orange solid (0.12 g, 0.008 mmol, 32%). ^{1}H NMR (C_6H_6): δ = 6.90 (s, 72H, Ar−H), 3.37 (s, 144H, CH_2N), 2.57 (s, 432H, $N(CH_3)_2$), 1.75 (br, $SiCH_2CH_2-$), 1.10 (br, $-CH_2SiMe_2-$), 0.95 (br, $SiCH_2CH_2-$), 0.49 (s, 216H, $Si(CH_3)_2$). MALDI-TOF-MS: *m*/*z* 5000−15000 (very broad peak). Anal. Calcd for 79% nickelated $C_{660}H_{1176}N_{72}Si_{53}Ni_{36}Cl_{36}$: C 56.05, H, 8.44, N 7.13, Ni 11.13. Found: C 55.65, H 8.28, N 6.22, Ni 11.33%.

[$NiCl_2$(C_6H_2{CH_2NMe_2}$_2$-2,6-($SiMe_3$)-4)] (16). To an orange-colored solution of **2** (96.8 mg, 0.271 mmol) in CH_2Cl_2 (25 mL) was added an excess of CCl_4 (∼5 mL). Instantaneously, a dark brownish solution was obtained, and the mixture was stirred for 16 h. After evaporating the solvent in vacuo and recrystallization from CH_2Cl_2/pentane, dark red to purple crystals were isolated which were suitable for an X-ray molecular structure determination. Yield: 42.2 mg (0.107 mmol, 40%). ESR (0.5 mg/mL in toluene glass at 150 K): g_x = 2.3879, g_y = 2.2009, g_z = 2.0261 (hyperfine coupling: 28 G). FAB-MS: *m*/*z* 391.1 (M^+). Anal. Calcd for $C_{15}H_{27}N_2SiNiCl_2$: C 45.83, H 6.92, N 7.13. Found: C 45.79, H 6.96, N 7.06%.

Electrochemical Measurements. All experiments were performed in an electrochemical cel where a nitrogen atmosphere was maintained. The measurements were made with a conventional three-electrode configuration using platinum electrodes and a Ag/AgCl reference electrode. Cyclovoltammetric studies were carried out in CH_3CN solutions containing the supporting electrolyte (0.1 M [Bu_4N]Cl). The reference electrode was separated from the test solution by a glass frit. Under the experimental conditions, $E_{1/2}$ for (Fc/ Fc^+) = +0.053 V (ΔE_p ≈ 80−100 mV). An EG&G potentiostat/galvanostat model 263A was used connected to model 270/250 Research Electrochemistry Software (version 4.23). Cyclic voltammograms were obtained with a scan rate of 100 mV s^{-1}.

Standard Catalytic Protocol. Prior to use, a mixture of MMA (28 mmol), CCl_4 (104 mmol) and dodecane (internal standard, 8.9 mmol) was degassed thoroughly using the freeze−pump−thaw method. Then the catalyst (∼9.1 × 10^{-5} mol) in CH_2Cl_2 (∼10 mL) was added at RT under an inert atmosphere. The reaction was monitored by withdrawing GC-samples at regular time intervals.

Membrane Experiments. All experiments were carried out at 25 °C in a 3.75 mL or a 10 mL polypropylene membrane reactor under an inert Argon atmosphere (Argonbox) using the standard catalytic protocol. The applied nanofiltration membrane (SelRO-MPF-50) was conserved in a aqeous solution of glycerine bisulfite, washed with acetone and conserved in acetone for 24 h *prior to* use.

X-ray Crystal Structure Determination of 16. $C_{15}H_{27}N_2SiNiCl_2$, M_r = 393.09 g/mole, dark red plate, 0.38 × 0.30 × 0.05 mm^3, monoclinic, $P2_1/c$ (no. 14), a = 9.9622(2) Å, b = 12.8152(3) Å, c = 15.5640(3) Å, β = 106.7933(14)°, V = 1902.28(7) $Å^3$, Z = 4, ρ = 1.373 g/cm^3. 13584 reflections were measured on a Nonius Kappa CCD diffractometer with rotating anode (λ = 0.71073 Å) at a temperature of 150(2) K. 4354 reflections were unique (R_{int} = 0.0421). Absorption correction with PLATON[38] (multiscan, μ = 1.359 mm^{-1}, 0.53−0.59 transmission). Structure solved with Patterson methods (DIRDIF97[39]) and refined with SHELXL97[40] aganist F^2 of all reflections. Non-hydrogen atoms were refined freely with anisotropic displacement parameters. Hydrogen atoms were located in the difference Fourier map and refined freely with isotopic displacement parameters. 298 refined parameters, *R*-values [$I > 2\sigma(I)$]: $R1$ = 0.0272, $wR2$ = 0.0648. *R*-values [all refl.]: $R1$ = 0.0392, $wR2$ = 0.0694. Molecular illustration, structure checking and calculations were performed with the PLATON package.[38] (See for further details the Supporting Information).

Acknowledgment. We are indebted to Cees Versluis from the Analytical Chemistry Department of the Utrecht University for FAB-MS measurements. A.W.K., M.L., and A.L.S thank the Council for Chemical Sciences (CW) and The Netherlands Organization for Scientific Research (NWO) for financial support.

Supporting Information Available: A listing of tables of atomic coordinates, bond lengths and angles, thermal parameters and relevant crystallographic data for compound **16**, Figure 3 (MALDI-TOF-MS analysis of **15**), a complete list of experimental procedures and analytical data for compounds **1**−**5** and **8**−**15** (PDF). This material is available free of charge via the Internet at http://pubs.acs.org.

JA0026612

(38) Spek, A. L. *PLATON*, a multipurpose crystallographic tool, Utrecht University, The Netherlands, 1998.

(39) Beurskens, P. T.; Admiraal, G.; Beurskens, G.; Bosman, W. P.; Garcia-Granda, S.; Gould, R. O.; Smits, J. M. M.; Smykalla, C. *The DIRDIF97 program system*, technical report of the crystallographic laboratory; University of Nijmegen, The Netherlands, 1997.

(40) Sheldrick, G. M. *SHELXL97*, program for crystal structure refinement; University of Göttingen, Germany, 1997.